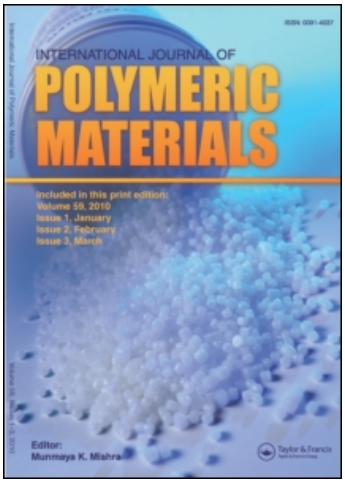


International Journal of Polymeric Materials
Publication details, including instructions for authors and subscription information:
http://www.informaworld.com/smpp/title~content=t713647664

# Linear and Nonlinear Viscoelastic Functions for Polymer Melts and Concentrated Solutions

G. A. Alvarez[a]; H. -J. Cantow[a]
[a] Institut für Makromolekulare Chemie der Universität-Freiburg, Freiburg i. Br., Federal Republic of Germany

**To cite this Article** Alvarez, G. A. and Cantow, H. -J.(1983) 'Linear and Nonlinear Viscoelastic Functions for Polymer Melts and Concentrated Solutions', International Journal of Polymeric Materials, 10: 1, 53 — 76
**To link to this Article: DOI:** 10.1080/00914038308077990
**URL:** http://dx.doi.org/10.1080/00914038308077990

*Intern. J. Polymeric Mater.*, 1983, Vol. 10, pp. 53–76
0091–4037/83/1001–0053 $18.50/0

Printed in Great Britain

# Linear and Nonlinear Viscoelastic Functions for Polymer Melts and Concentrated Solutions

G. A. ALVAREZ and H.-J. CANTOW

*Institut für Makromolekulare Chemie der Universität-Freiburg, Stefan-Meier-Straße 31, 7800 Freiburg i. Br., Federal Republic of Germany*

(*Received September 1, 1982*)



Recent modifications of the Rouse theory for polymer melts and concentrated solutions are presented and compared with measurements of dynamic modulus and oscillatory first normal stress coefficients for cis-1,4-polybutadiene (PB). Measurements of finite-amplitude storage modulus and second normal stress coefficient are given alongside with current theories aimed to explain these effects. Nonlinear transient measurements for PB melts, although in some cases impeded by instrument compliance, provide critical test for theory. The procedure of extending results of the network theory to nonlinear behaviour, as exemplified by Carreau's model is shortly reviewed. It can be concluded that molecular theories based on clear, independently testable assumptions of molecular architecture, are likely to be better guides for progress in polymer dynamics, than empirical theories.

## INTRODUCTION

Polymer melts are characterized by extreme deviations from linear viscoelastic behaviour. There are two competing theories that may explain the myriad of complicated results observed in polymer melts and concentrated systems: Lodge's network theory[1] based on the kinetic theory of rubber elasticity, in which chemical crosslinks are replaced by temporary physical entanglements, and the Doi and Edwards theory[2] which considers reptation or curvilinear diffusion of a single chain along its own contour as the main molecular motion. Recently, Curtiss and Bird[3] have developed a kinetic theory with constraints on bond angles and bond lengths and have also rederived the Doi and Edwards theory without conceptual frames like tubes, slip-links or Maxwell demons of the Doi and Edwards theory.

In the limit of linear viscoelasticity the Rouse theory, which is identical to the linear network theory, or the generalized Maxwell model, although with

different meanings to the parameters involved, has served the traditional role of explaining in molecular terms the behaviour of polymers, particularly the frequency dependence of linear viscoelastic functions for polymers in dilute solution.

In this paper we review the achievements of the linear theory and present some results on nonlinear viscoelastic functions and the theories aimed to explain them, in order to bring into perspective the vast source of molecular information available in polymer dynamics.

## THE GENERALIZED MAXWELL MODEL

The simplest rheological equation containing the notions of viscosity and elasticity is the Maxwell model. A superposition of Maxwell models may be written:[4]

$$\tau = \sum_{p=1}^{\infty} \tau_p \tag{1}$$

$$\tau_p + \lambda_p \frac{\partial \tau_p}{\partial t} = -\eta_p \gamma \tag{2}$$

where $\tau$ is the stress tensor, $\gamma$ here the infinitesimal strain tensor and $\lambda_p$ and $\eta_p$ are scalars with dimensions of time and viscosity respectively.

The Rouse theory[5] gives expressions for $\lambda_p$ and $\eta_p$ in terms of molecular constants, by idealizing the polymer molecule as composed of $N+1$ identical Stokes beads connected by $N$ identical Gaussian springs. The results are:

$$\eta_p = ckT\lambda_p \tag{3}$$

$$\lambda_p = \frac{f_0 b^2 N^2}{6\pi^2 p^2 kT} \tag{4}$$

$f_0$ is the bead friction coefficient, $b$ is the root-mean-square end-to-end distance for two adjacent beads at equilibrium, and $c$ is the number of molecules per unit volume. The solution of Eq. (2) gives for small-amplitude oscillatory motion, neglecting solvent contribution:

$$i\omega\eta^*(\omega) \equiv G^*(\omega) = ckT \sum_{p=1}^{N} \frac{i\omega\lambda_p}{1+i\omega\lambda_p} \tag{5}$$

where $\eta^*$ is the complex viscosity and $G^*$ is the complex modulus. Normal stresses cannot be obtained from this model, inasmuch as normal stresses are nonlinear effects.

The development of nonlinear constitutive equations requires, among other

things, that the equations do not depend on local fluid rotation. A coordinate frame rotating and translating with the fluid is named corotational. Reformulation of the Maxwell model in a corotational frame yields the following nonlinear material functions:

$$\Psi_1^d = ckT \sum_{p=1}^{N} \frac{\lambda_p^2}{1+(\omega\lambda_p)^2} \tag{6}$$

$$\Psi_1^* = ckT \sum_{p=1}^{N} \frac{\lambda_p^2}{(1+i\omega\lambda_p)(1+2i\omega\lambda_p)} \tag{7}$$

where $\Psi_1^d$ is the first normal displacement stress coefficient and $\Psi_1^*$ is the complex first normal stress coefficient.

These results apply strictly to an isolated macromolecule. To simulate polymer-polymer interactions in concentrated systems Ferry[6] proposed a modification of the Rouse theory consisting of two sets of relaxation times corresponding to motions below and above the critical length for the onset of entanglements characterized by $M_C$, the molecular weight at which the zero-shear viscosity changes from its linear dependence on molecular weight to a 3.4 power law on molecular weight. We have found that a smooth transition between the two regimes of relaxation times, namely

$$\lambda_{p_{\text{mod}}} = \lambda_p p_e^{2.4\exp(-p/p_e)} \tag{8}$$

where $p_e$ is the critical mode index

$$p_e = M/M_C \tag{9}$$

agreed better with experiment than the traditional sharp transition.[7]

On the contrary, the Doi and Edwards prediction

$$G^*(\omega) = G_N^0 \sum_{p,\text{odd}} \frac{8}{p^2\pi^2} \frac{i\omega\lambda_p}{1+i\omega\lambda_p} \tag{10}$$

$$\lambda_p = \frac{f_0 b^2 N^2 M}{\pi^2 p^2 kTM_e}, \quad M_C \simeq 2M_e \tag{11}$$

implies an extremely sharp transition into the plateau region, in disagreement with experiment, as will be shown below. The smooth transition might be attributed to fluctuations in the critical molecular weight parameter $M_C$.

## EFFECT OF MOLECULAR WEIGHT DISTRIBUTION

In order to compare theoretical results with experiments on real polymers it is necessary to have a measure of the effect of molecular weight distribution on

the experiment. This can be achieved in principle by integration over the molecular weight distribution, when the molecular weight is stated explicitly in the equations. We prefer to adopt an empirical approach which is known to agree better with experiment.[8]

A phenomenological $n$th-order law for the blending of $q$ species, each of weight fraction $w_i$, can be written, after Kurata *et al.*[9]

$$H\left(\frac{n}{q}\right) = \left\{\sum_{i=1}^{q} w_i \left[H_i\left(\frac{\lambda}{k_i}\right)\right]^{1/n}\right\}^n \tag{12}$$

where

$$H_i(\lambda) = h(\xi); \quad \xi = \frac{\lambda}{\left(\prod_{i=1}^{q} \lambda_{m_i}\right)^{1/q}} \tag{13}$$

$H(\lambda)$ is the distribution function of relaxation times $\lambda$ and $\lambda_m$ is the longest relaxation time. $H$ is defined by the transform of

$$\eta^* = \int_0^\infty \frac{\lambda H(\lambda)\, \mathrm{d}\lambda}{1 + i\omega\lambda} \tag{14}$$

but is usually obtained numerically. The following limits exist:

$$\eta_0 = \lim_{\omega \to 0} \eta'(\omega) = \int_0^\infty H(\lambda)\, \mathrm{d}\lambda \tag{15}$$

$$\Psi^d_{1_0} = \lim_{\omega \to 0} \frac{\eta''(\omega)}{\omega} = \int_0^\infty H(\lambda)\lambda\, \mathrm{d}\lambda \tag{16}$$

The shift factors $k_i$ are given by

$$k_i = \left(\frac{M_w}{M_i}\right)^{3.4-n} \tag{17}$$

where the empirical law for the zero-shear viscosity of the blend

$$\eta_{0_b} \propto M_w^{3.4} \tag{18}$$

is assumed. (Cf. Doi and Edwards $\eta_{0_{dis}} \propto M_w M_z M_{z+1}$.)

## EXPERIMENTAL RESULTS AND CALCULATIONS

The material referred to as the PB melt in the following, consisted of a 97% cis-, 1.5% 1,2-, 1,4-polybutadiene with molecular weights in kg mol$^{-1}$

| $M_n$ | $M_w$ | $M_z$ | $M_{z+1}$ |
|---|---|---|---|
| 218 | 488 | 1078 | 1942 |

obtained from gel permeation chromatography and light scattering measurements.

Figure 1 presents the storage modulus *vs.* frequency for the PB melt and a 24% solution of PB in n-tetradecane, measured in the Instron 3250 Rheometer with Eccentric Rotating Disc geometry, referred to 298 K and melt density according to standard procedures.[10] Measurements were corrected for instrument compliance and inertia. The broken line represents calculations from the monodisperse Rouse theory with smooth transition. The solid line was calculated by blending of spectra according to the cubic law, for 3 species of molecular weights aimed to match the first five moments of the molecular weight distribution of PB. The spectra were obtained from Rouse storage

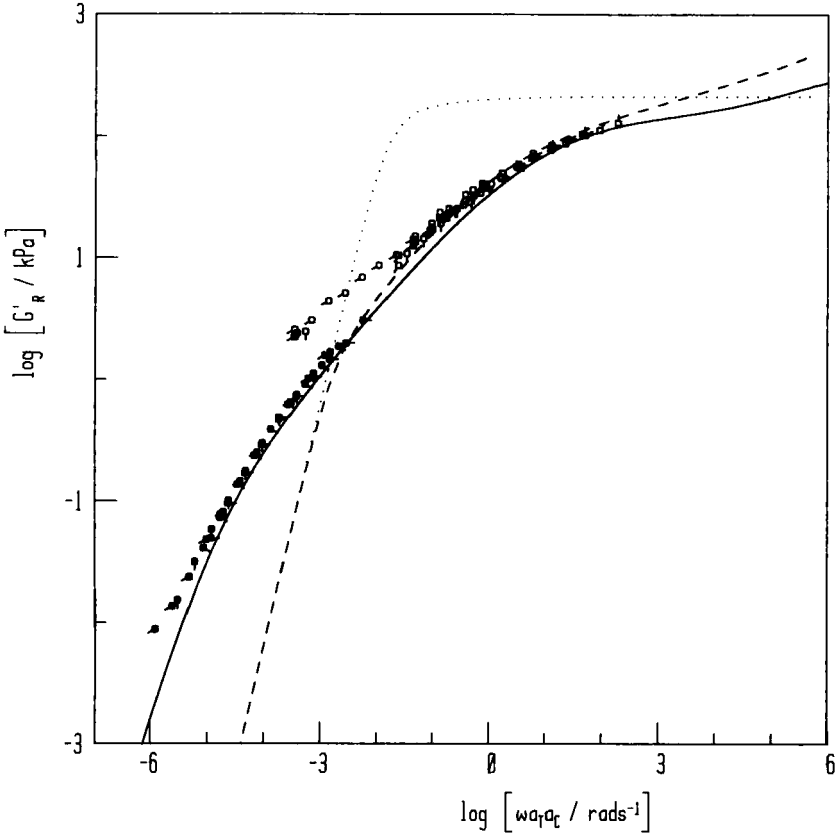


FIGURE 1 Storage modulus *vs.* frequency masterplot for PB melt ○ and 24% solution in n-tetradecane ● measured in the Eccentric Rotating Disc (ERD) geometry and reduced to 298 K and 918 kg mol$^{-1}$ melt density. ——— Rouse theory with heterodispersity correction; – – – – Rouse theory with M = 488 kg mol$^{-1}$; ····· Doi–Edwards theory.

moduli by means of Tschoegl's third order approximation[11] and then refined iteratively. The Doi and Edwards prediction is given by the dotted line, and shows that a sharp transition to the rubber plateau is inadequate to reproduce the experiment.

The loss modulus measured in the same experiment as Figure 1 is shown in Figure 2, where it can be seen that the loss modulus or the dynamic viscosity $\eta' = G''/\omega$ are not very sensitive to the molecular weight distribution. The inadequacy of the Doi and Edwards model is even more accentuated in this plot that shows that $\lim_{\omega \to \infty} G'' = 0$ is unrealistic.

The shear and normal stresses measured in cone-and-plate oscillatory strain are displayed in Figure 3 for the PB melt, a 24% solution of PB in n-tetradecane and a PB oil of $M_n = 6$ kg mol$^{-1}$ before inertia correction. The points are digitized amplifier signals and the lines are sine waves with

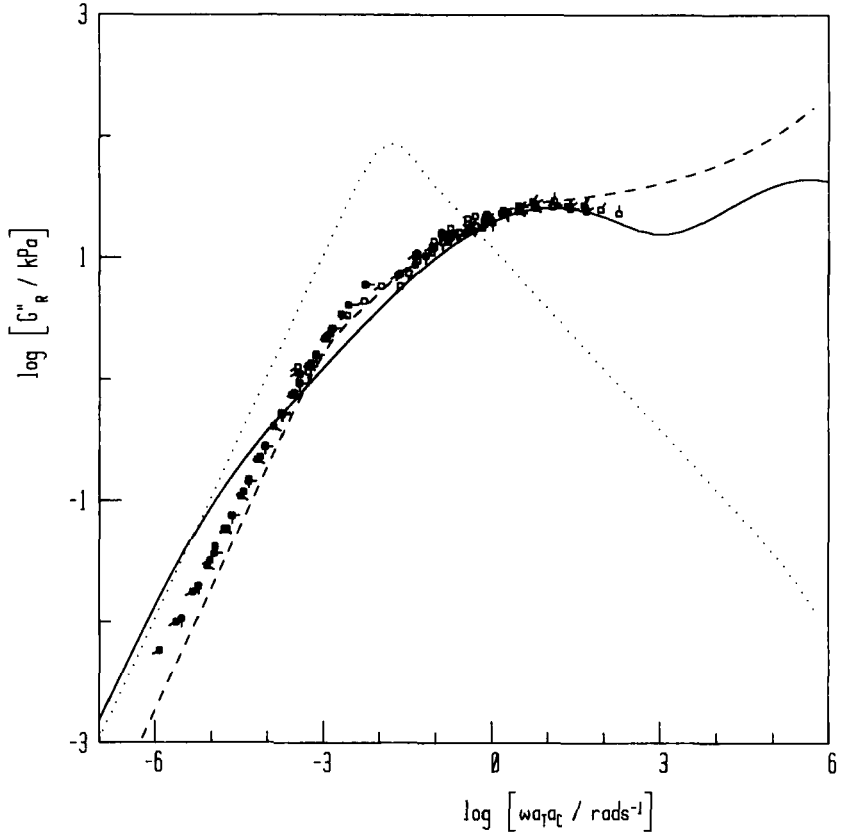


FIGURE 2 Loss modulus as in Figure 1.

optimized amplitude and phase to match the experiment. The shear phase angles are seen to vary from near 0 for the melt to nearly $\pi/2$ for the oil. The normal forces oscillate at twice the shear frequency and are positively displaced for sufficiently small inertia effects. Twice the normal phase angle lies between the third and fourth circle quadrant and hence the in-phase component of the complex first normal stress difference may exhibit a change of sign. The displacement and out-of-phase first normal stress coefficients calculated with inclusion of inertia[12] are plotted in Figures 4 and 5 for the PB melt, a 24% solution of PB in PB oil ($M_n = 1.5\ \text{kg mol}^{-1}$) and a 24% solution of PB in n-tetradecane. The theoretical curves are results from the monodisperse (broken lines) and polydisperse (solid lines) Rouse theory. It is clearly seen that, compared to the dynamic viscosity, the first normal stress coefficients are very sensitive to molecular weight distribution, in the terminal region of the spectra. However, only the n-tetradecane solutions agree well with theory; there is no explanation at present for the discrepancy.

To our knowledge, this is the first time oscillatory normal stress coefficients are measured for melts. A single frequency demonstration has been given by Meissner.[18]

The zero-shear viscosity and zero-shear first normal displacement stress coefficient for the modified Rouse theory are given by:

$$\eta_0 = \frac{cf_0 b^2 N^2}{6\pi^2} \sum_{p=1}^{N} \frac{p_e^{2.4\exp(-p/p_e)}}{p^2} \tag{19}$$

$$\Psi^d_{1_0} = \frac{cf_0^2 b^4 N^4}{36\pi^4 kT} \sum_{p=1}^{N} \frac{p_e^{4.8\exp(-p/p_e)}}{p^4} \tag{20}$$

Measurements of the zero-shear viscosity for 3 PB oils ($M_n = 1.5$, 3 and 6 kg mol$^{-1}$) and first normal displacement stress coefficient for one PB oil ($M_n = 6$ kg mol$^{-1}$) are presented in Figure 6 *vs.* weight average molecular weight, alongside with calculations from the monodisperse Rouse theory and from the molecular weight heterogeneity correction with $n = 1$ below and $n = 3$ above $M_C$. The smooth transition from $\eta_0 \propto M_w$ to $\eta_0 \propto M_w^{3.4}$ can also be seen in the plot. No theory is known to have the property of bridging viscoelastic functions below and above $M_C$.

## FINITE-AMPLITUDE STORAGE MODULUS

The results in previous paragraphs all share a common property of being limiting behaviour at infinitesimal strain. We present results now where the stress is finite.

The storage modulus of the PB melt measured in cone-and-plate oscillatory

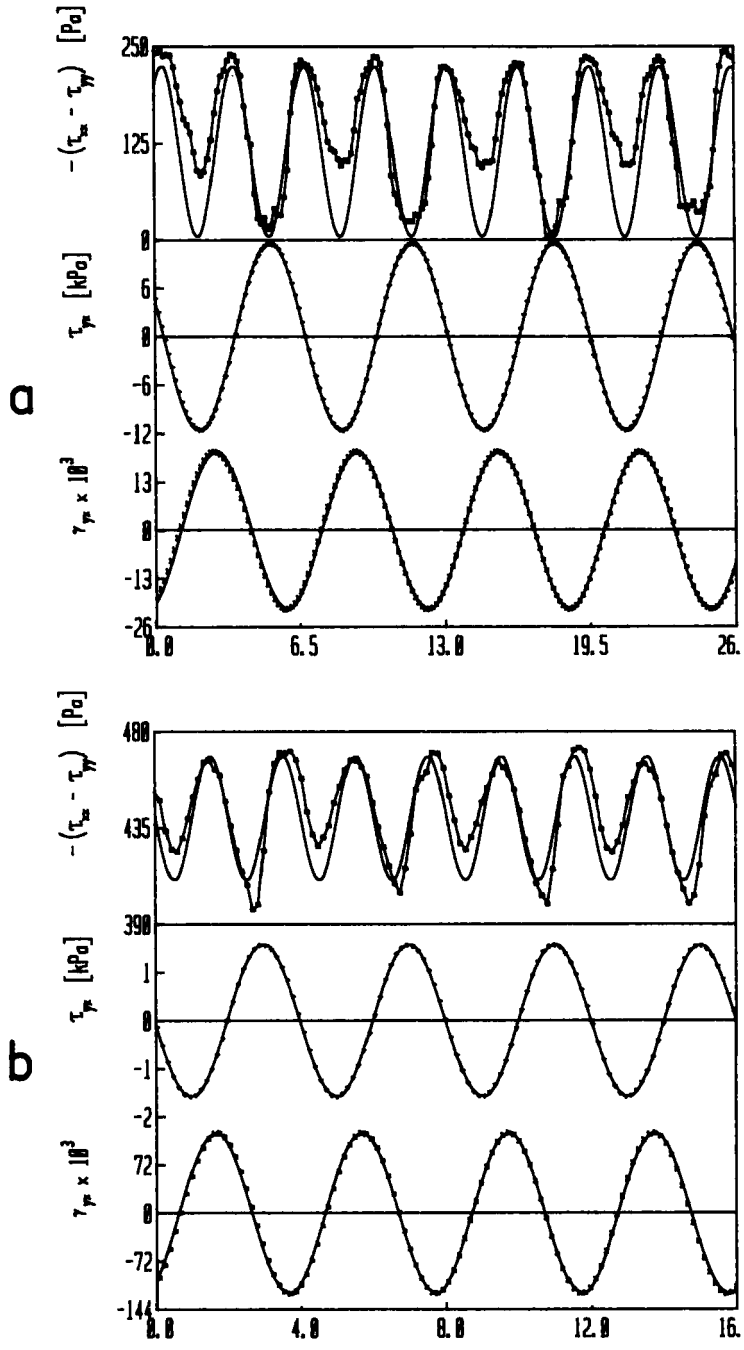

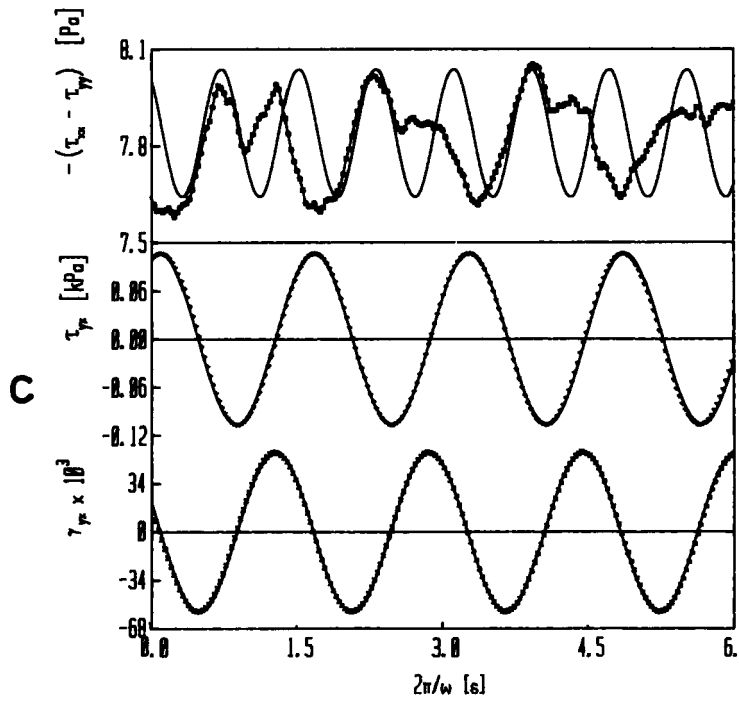


FIGURE 3 Oscillatory input shear strain and output shear and normal stress in cone-and-plate geometry: a) PB melt, b) a solution of PB (24%) in n-tetradecane, c) a PB oil with $M_n$ = 6 kg mol$^{-1}$. Points are digitized amplifier signals and lines are sine functions fitted to the experimental data.

a) Melt ($M_w$ = 488 kg mol$^{-1}$)

| | |
|---|---|
| Temperature | 352 K |
| Frequency | 0.996 rad s$^{-1}$ |
| Strain amplitude | 20.94 mrad |
| Cone angle | 105 mrad |
| Plate diameter | 40 mm |

b) 24 % soln. in n-tetradecane

| | |
|---|---|
| Temperature | 313 K |
| Frequency | 1.578 rad s$^{-1}$ |
| Strain amplitude | 209.4 mrad |
| Cone angle | 105 mrad |
| Plate diameter | 60 mm |

c) Oil ($M_n$ = 6 kg mol$^{-1}$)

| | |
|---|---|
| Temperature | 298 K |
| Frequency | 1.578 rad s$^{-1}$ |
| Strain amplitude | 52.36 mrad |
| Cone angle | 21 mrad |
| Plate diameter | 60 mm |

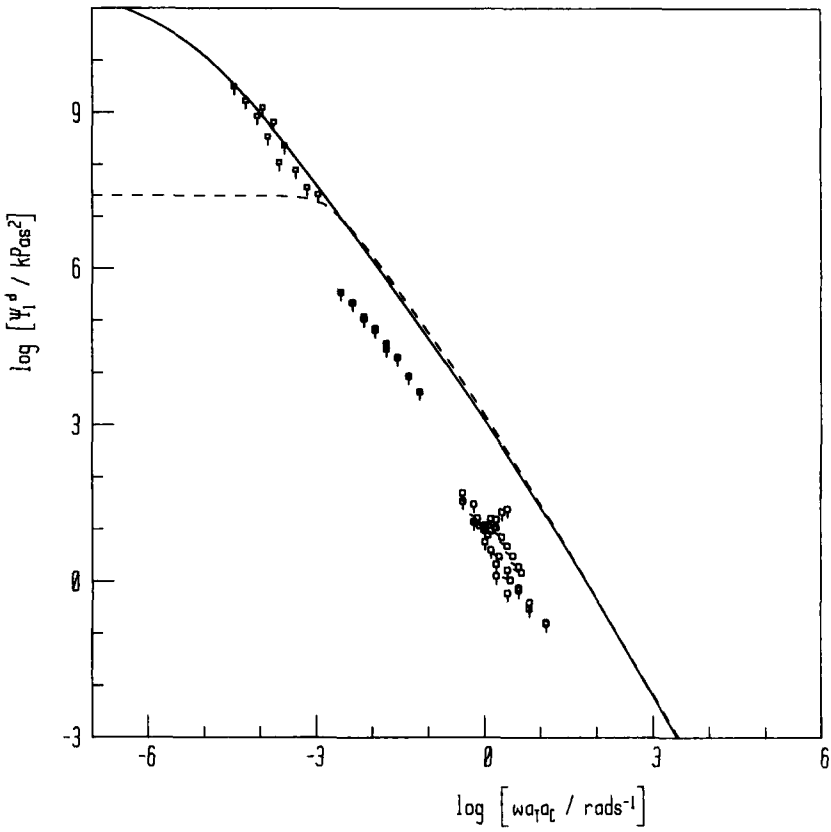


FIGURE 4 First normal displacement stress coefficient *vs.* frequency masterplot for PB melt ○, a 24% solution of PB in PB oil of $M_n = 1.5\,\text{kg mol}^{-1}$ ● and a 24% solution of PB in n-tetradecane □ measured in cone-and-plate oscillatory motion and reduced to 298 K and 918 kg $\text{mol}^{-1}$ melt density. ——— Rouse theory with heterodispersity correction; – – – – Rouse theory with $M = 488\,\text{kg mol}^{-1}$.

shear *vs.* strain is given in Figure 7. The extreme sensitivity of the nonlinear storage modulus to the frequency is however, surprising, and could be an artifact of the experimental conditions. For comparison, the results of the rigid dumbbell theory[13] as well as a recent extension of the Doi and Edwards theory by Pearson[24] are shown in Figure 8. Limiting frequencies, which must necessarily exist, are of the order of 0.02 and 0.4 rad $\text{s}^{-1}$ for the two theories. Our experiment on the other hand, does not show limit in frequencies up to 20 rad $\text{s}^{-1}$. There is no explanation for these results.

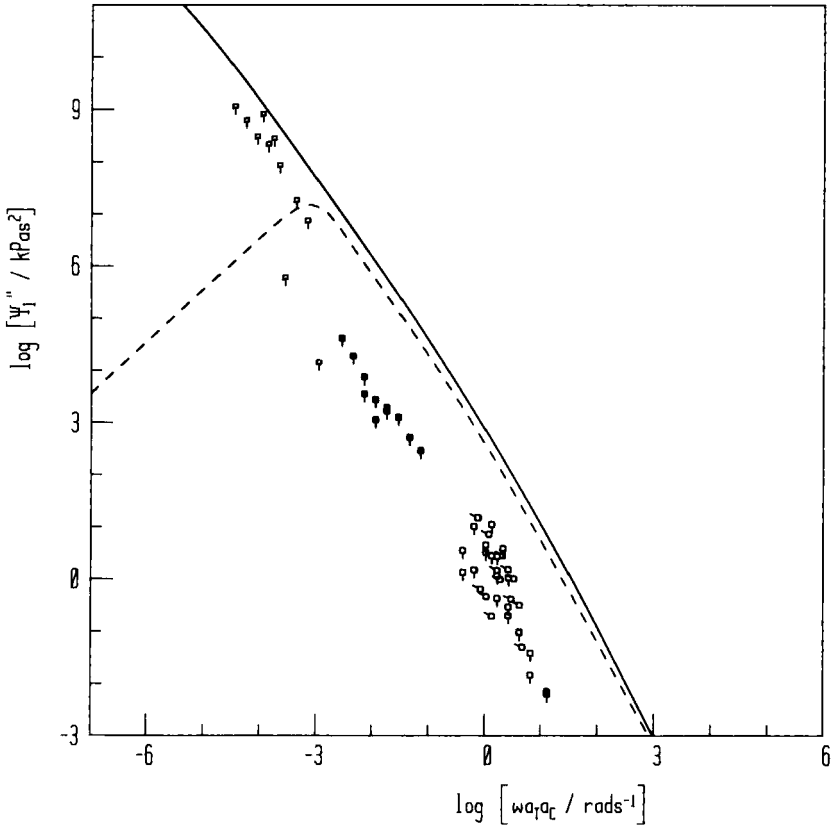


FIGURE 5 First normal out-of-phase stress coefficient as in Figure 4.

## SECOND-NORMAL STRESS DIFFERENCE

Another manifestation of nonlinear viscoelastic behaviour in polymers of extreme theoretical and practical interest is the second normal stress coefficient.

It has been claimed[15] that the total thrust in the eccentric rotating disc experiment gives a measure of the second normal stress coefficient. Such measurement is straightforward provided sensitive electronics are at hand to record very weak signals.

The slopes of linear plots of normal stress *vs.* square of strain are given in Figure 9 *vs.* angular frequency for the PB melt, including inertia correction. A change of sign in this function is apparent. Here a positive stress-*vs.*-square-strain slope indicates a tendency of the plates to be pushed apart and hence a

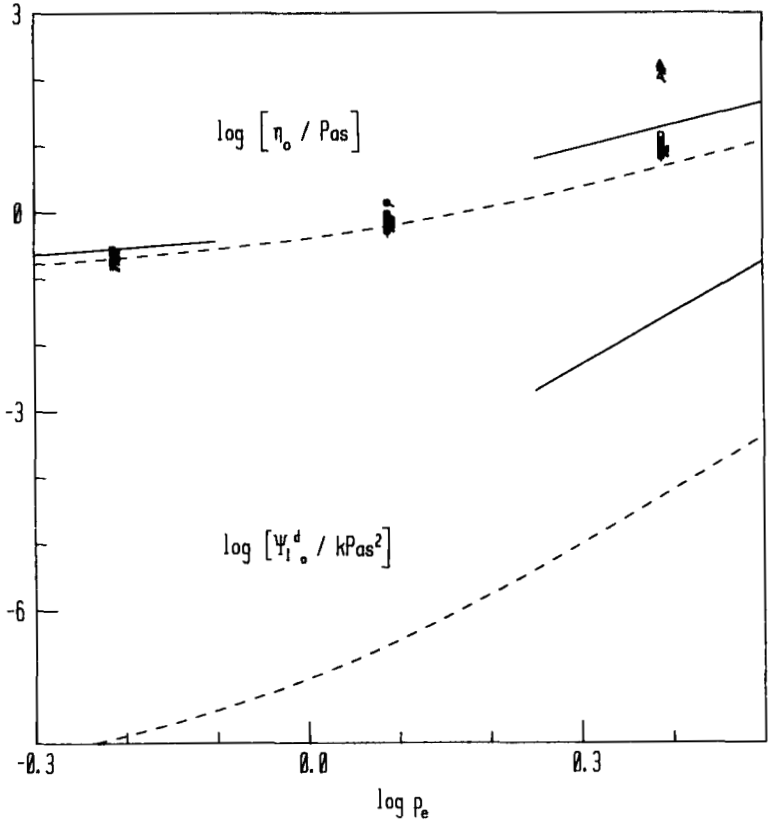


FIGURE 6 Zero-shear viscosity ● and zero-shear first normal displacement stress coefficient △ *vs.* weight average molecular weight for PB oils with $M_w = 3$, 6 and 12 kg mol$^{-1}$. ——— Heterodisperse Rouse theory with $n = 1$ below and $n = 3$ above $M_C$; — — — Monodisperse Rouse theory with smooth transition from $\eta \propto M$ to $\eta \propto M^{3.4}$.

negative second normal stress coefficient by definition. The negative of the second normal stress coefficient, omitting positive points, is compared with the first normal stress coefficient measured in cone-and-plate geometry, in Figure 10. Thus, the second normal stress coefficient appears to have a stronger shear rate dependence than the first normal stress coefficient.

Models predicting a stronger shear rate dependence for the second normal stress coefficient exist; the power law asymptotes for $\lambda_h\dot{\gamma} \to \infty$ in the rigid dumbbell model for dilute solutions, are given by:[13]

$$\frac{\eta - \eta_s}{nkT\lambda_h} = 0.678\,\frac{1-h}{1-2h}\,(\lambda_h\dot{\gamma})^{-1/3} \tag{21}$$

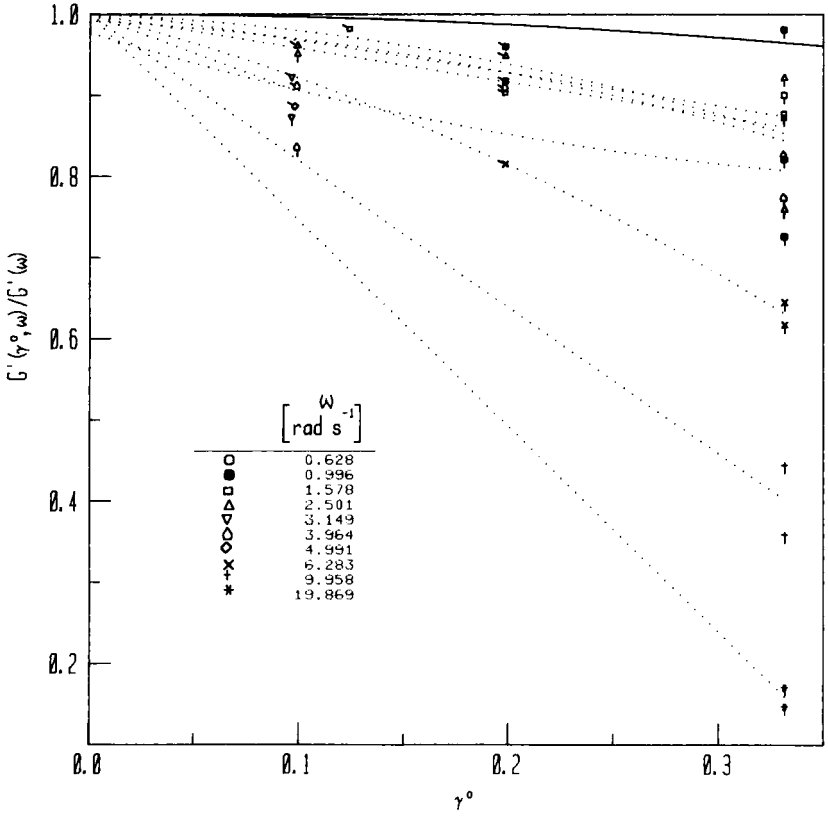


FIGURE 7 Finite-amplitude storage modulus *vs.* peak strain for PB melt in frequency range 0.6–20 rad $s^{-1}$. ····· fit to square law; ——— Doi–Edwards theory at $\omega = \infty$.

$$\frac{\Psi_1}{nkT\lambda_h^2} = 1.2\frac{1-h}{1-2h}(\lambda_h\dot{\gamma})^{-4/3} \tag{22}$$

$$\frac{\Psi_2}{nkT\lambda_h^2} = 0.93\frac{h}{1-2h}(\lambda_h\dot{\gamma})^{-7/3} \tag{23}$$

where $h$ is a parameter indicating the degree of hydrodynamic interaction.

Thus, the second normal stress coefficient is positive and vanishes in the absence of hydrodynamic interaction. Bird and Curtiss have recently shown[21] that for rigid rodlike molecules $\Psi_2$ is positive for models with less than 5 beads and negative for models with 5 beads or more.

Similarly, shear rate powers for melts, obtained by Curtiss and Bird are:[16]

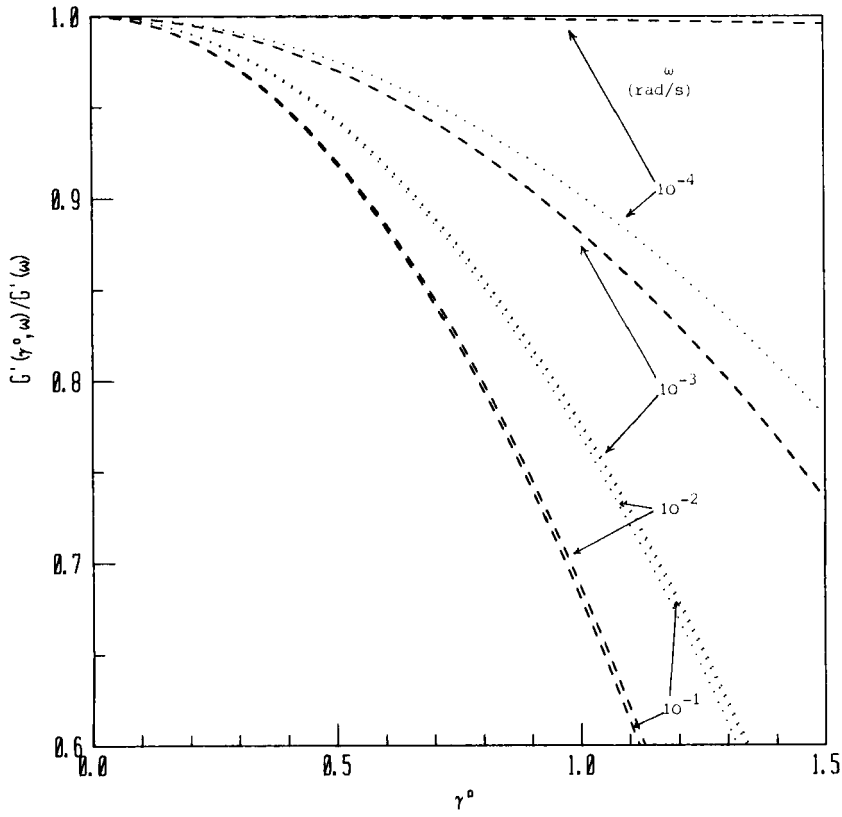


FIGURE 8 Theoretical predictions of finite-amplitude storage modulus *vs.* peak strain, according to rigid dumbbell ····· and Doi–Edwards — — — theory for frequency range $10^{-4}$–$10^{-1}$ rad $s^{-1}$.

$\Psi_1/NnkT\lambda^2 \to 2\varepsilon \ln \lambda\dot{\gamma}(\lambda\dot{\gamma})^{-2}$ and $\Psi_2/NnkT\lambda^2 \to -1.1619(1-\varepsilon)(\lambda\gamma)^{-5/2}$. The shear rate powers for $\eta$ and $\Psi_1$ in Eqs (21) and (22) agree well with the experiments shown below, Figure 12, and the exponent of the power law for $\Psi_2$ in Figure 10 is $\sim 2$.

## STEP-STRAIN SHEAR AND NORMAL STRESS RELAXATION

It is known that the dynamic viscosity and first normal stress coefficients do not provide a critical test for the evaluation of rheological models. Better test can be obtained from measurements of time-dependent functions. Such measurements, however, place severe limitations on instrument performance

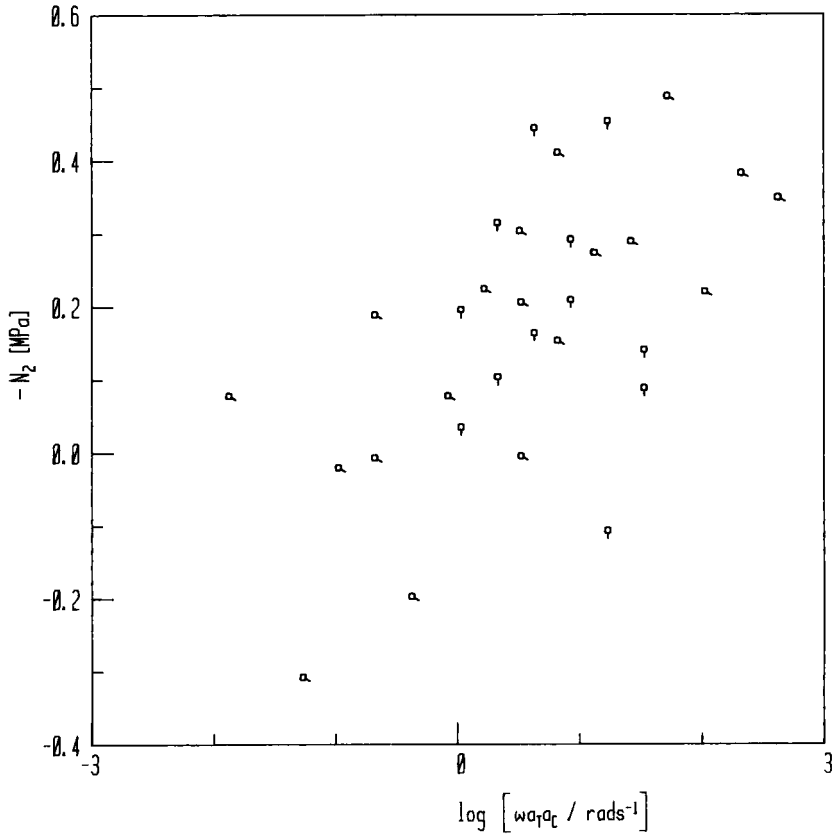


FIGURE 9 Second normal stress difference *vs.* frequency measured in ERD geometry for PB melt.

and care must be taken to interpret experiments, as shown below.

Figure 11 shows shear and normal stress relaxation after a sudden shear strain for the PB melt on the Instron 3250 Rheometer in cone-and-plate geometry at 298 K. The cone angle was 6° and the plate diameter was 20 mm. The broken line is the stress relaxation modulus calculated from the Rouse theory with smooth transition into the plateau region and the dotted line is calculated by the same theory with a sharp transition. The shear strain was around 1, and two consecutive experiments on the same sample are shown.

For a wide class of constitutive equations including Lodge's network model:

$$\tau(t) = \int_{-\infty}^{t} m(t, t')\gamma_{[0]}(t, t')\, dt' \tag{24}$$

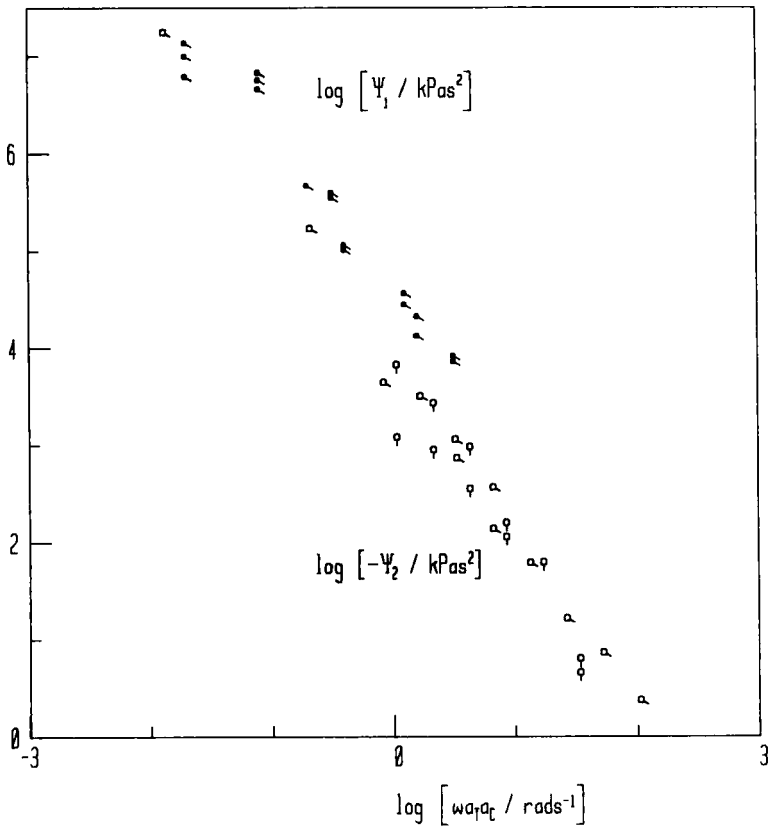


FIGURE 10 Comparison of first normal stress coefficient measured in cone-and-plate oscillatory motion and negative of second normal stress coefficient (positive points excluded) measured in ERD geometry for PB melt.

where the stress $\tau$ is related to the material memory function $m(t, t')$ and to the contravariant finite-strain tensor. For simple shear in the 1,2 plane a simple relationship exists between three components of $\gamma_{[0]}$ referred to a Cartesian coordinate system, namely

$$\gamma_{[0]11} - \gamma_{[0]22} = \gamma\gamma_{[0]12} \tag{25}$$

where $\gamma$ is the amount of shear. Assuming that during the time of shear the network connectivity does not change, then

$$\tau_{11} - \tau_{22} = \gamma\tau_{12} \tag{26}$$

at any instant along the time axis. The relationship (25) is valid also for any isotropic function $\mathbf{I}(\gamma_{[0]})$ as follows directly from the definition of isotropy.

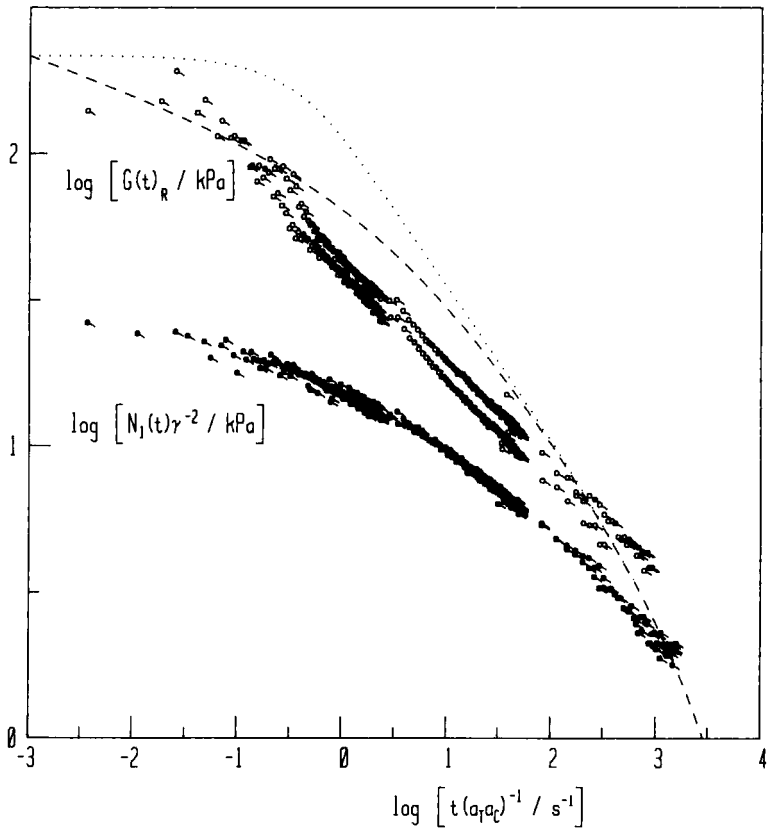


FIGURE 11 Shear and normal stress relaxation modulus *vs.* time for step strain experiment, $\gamma \simeq 1$, PB melt, 298 K. – – – Rouse theory with smooth transition into plateau regime and ····· Rouse theory with sharp transition. Two consecutive experiments separated by $t = \infty$ are shown.

According to Eq. (24), the two material functions plotted in Figure 11 must coincide and failure to do so could be attributed to instrument error.

Alternatively, the material does not obey Eq. (24). Other forms for constitutive equations have been given by Lodge.[19] The good agreement between the modified Rouse theory and the shear stress relaxation modulus in step strain, Figure 11, suggests that the instrument might be rigid enough for the torque measurements considered here.

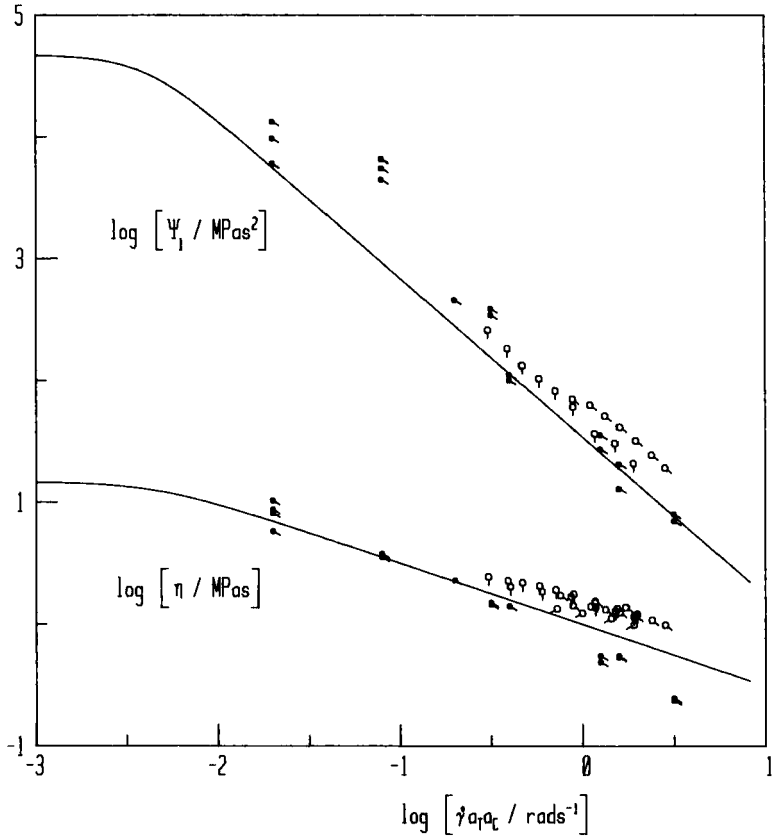


FIGURE 12 Steady-state viscosity and first normal stress coefficient *vs.* shear rate for PB melt, 298 K. Data are recovered from start of shear flow ○, cessation of shear flow ● and high shear rate viscosities from slit die rheometer □. Lines are predictions of Carreau model.

## TIME-DEPENDENT MATERIAL FUNCTIONS. COMPARISON WITH THE NETWORK MODEL

One of the most successful attempts up to date to modify empirically the network theory, is due to Carreau.[17] More recent attempts have been made by Acierno *et al.*,[20] but no explicit equations can be obtained from their theory. We first briefly discuss the linear theory.

Lodge's network theory[1] consists of a modification of the kinetic theory of rubber elasticity in which crosslinks are conceived as temporary junctions. The assumptions concerning the loss rate of junctions at time $t$ can be written:

$$\frac{\partial}{\partial t} n_{tt'p} + \lambda_p^{-1} n_{tt'p} = 0 \tag{27}$$

where $n_{tt'p}$ denotes the number of segments of type $p$ per unit volume created in time interval $t'$ to $t'+\mathrm{d}t'$. The integration of Eq. (27) yields the linear memory function:

$$n_{tt'}kT = \sum_p n_{tt'p}kT = kT\sum \frac{\eta_p}{\lambda_p^2}\,\mathrm{e}^{-(t-t')/\lambda_p} \tag{28}$$

with the initial condition:

$$n_{t't'p} = \frac{\eta_p}{\lambda_p^2} \tag{29}$$

Carreau[17] modified the linear memory function by allowing the junction creation rate $\eta_p/\lambda_p^2$ and the probability of loss of junctions $\lambda_p^{-1}$ to depend on the instantaneous value of the second invariant of the rate-of-strain tensor. The memory function becomes:

$$m(t,t',\mathrm{II}(t')) = kT\sum_p \frac{\eta_p f_p(\mathrm{II}(t'))}{\lambda_p^2}\exp\left[-\int_{t'}^{t}\frac{\mathrm{d}t''}{\lambda_p g_p(\mathrm{II}(t''))}\right] \tag{30}$$

where $f_p = g_p = 1$ as $\mathrm{II}\to 0$.

The following material functions are obtained:

$$\eta = \sum_{p=1}^{\infty}\eta_p f_p g_p^2 \tag{31}$$

$$\Psi_1 = 2\sum_{p=1}^{\infty}\eta_p\lambda_p f_p g_p^3 \tag{32}$$

$$\eta^+(\dot\gamma,t) = \eta(\dot\gamma) + \sum_{p=1}^{\infty}\eta_p\left\{\frac{t}{\lambda_p}(1-f_p g_p) - f_p g_p^2\right\}\mathrm{e}^{-t/\lambda_p g_p} \tag{33}$$

$$\Psi_1^+(\dot\gamma,t) = \Psi(\dot\gamma) + \sum_{p=1}^{\infty}\eta_p\left\{\frac{t^2}{\lambda_p}(1-f_p g_p) - 2t f_p g_p^2 - 2\lambda_p f_p g_p^3\right\}\mathrm{e}^{-t/\lambda_p g_p} \tag{34}$$

$$\eta^-(\dot\gamma,t) = \sum_{p=1}^{\infty}\eta_p f_p g_p^2\,\mathrm{e}^{-t/\lambda_p} \tag{35}$$

$$\Psi_1^-(\dot\gamma,t) = \sum_{p=1}^{\infty}\eta_p\lambda_p f_p g_p^3\,\mathrm{e}^{-t/\lambda_p} \tag{36}$$

where $\eta_p$ and $\lambda_p$ are given by analogy to the Rouse theory by:

$$\lambda_p = \frac{2^\alpha\lambda}{(p+1)^\alpha}, \qquad \eta_p = \eta_0\frac{\lambda}{\sum_{p=1}^{\infty}\lambda_p} \tag{37}$$

Second normal stress coefficients can be obtained by introduction of a new strain measure $(1-\varepsilon)\gamma_{[0]}-\varepsilon\gamma^{[0]}$ into the constitutive equation, where $\varepsilon$ is the ratio of the second to the first normal stress coefficient. The $f_p$ and $g_p$ functions of $\mathrm{II} = 2\dot{\gamma}^2$ were chosen by Carreau:

$$f_p = \frac{1+\left[\frac{1}{2}(2^{\alpha}t_1)^2\mathrm{II}\right]^S \Big/ (p+1)^{2\alpha}}{\left[1+\frac{c^2}{2}\lambda^2\mathrm{II}\right]^{2R}} \tag{38}$$

$$g_p = \frac{\left[1+\frac{c^2}{2}\lambda^2\mathrm{II}\right]^R}{1+\left[\frac{1}{2}(2^{\alpha}t_1)^2\mathrm{II}\right]^S \Big/ (p+1)^{2\alpha}} \tag{39}$$

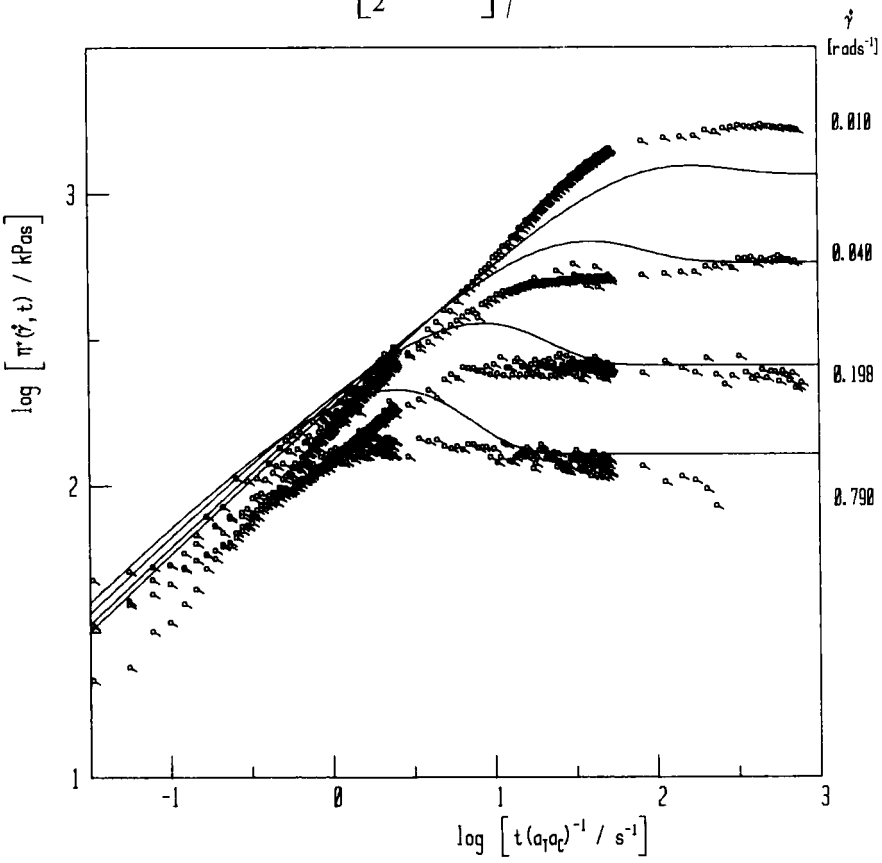


FIGURE 13 Viscosity at start of steady shear flow *vs.* time, PB melt, 298 K. Shear rate: 0.01–0.8 rad s$^{-1}$. Lines are predictions of Carreau model.

This choice of $f_p$ and $g_p$ gives for the steady-state viscosity a Cox–Merz type relationship and from it the value of $t_1$ may be obtained, thus

$$\eta(\dot{\gamma}) = \eta'\left(\frac{\lambda}{t_1}\omega\right) \tag{40}$$

The Rouse theory gives values of $S = 1$, $\alpha = 2$ and with $c = 1$ the only adjustable parameter left is $R$ which controls the exponent of the power law for the first normal stress coefficient.

Carreau's model was chosen here because it yields explicit material functions which revert easily to the linear limit.

Other modifications of the memory function are conceivable. In particular,

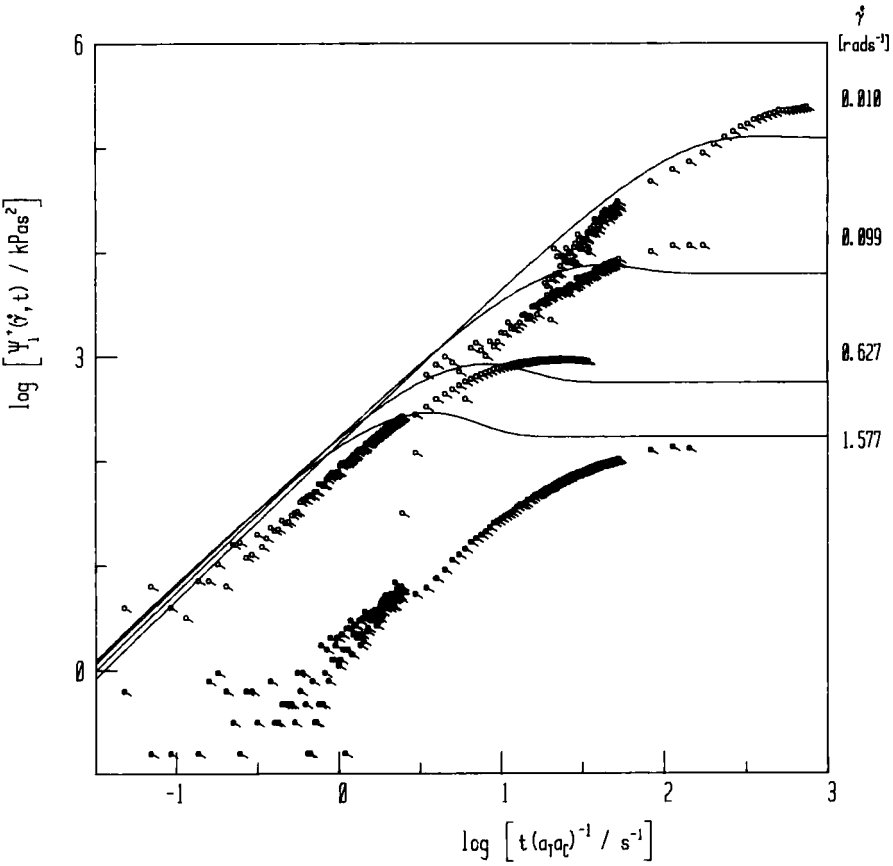


FIGURE 14 First normal stress coefficient at start of steady shear flow *vs.* time, PB melt, 298 K. Shear rate: 0.01–1.6 rad $s^{-1}$. Cone angle: 6 degrees, except data at 1.6 rad $s^{-1}$ where cone angle: 1.2 degrees. Lines are predictions of Carreau model.

stress overshoots can be obtained only for $f_p g_p < 1$. We do not consider further modifications of the memory function in this paper.

Figure 12 presents results for the steady-state viscosity and first normal stress coefficient for the PB melt at 298 K, recovered from start-up and cessation of steady shear flow, as well as measurements on a slit die rheometer. The lines are predictions of Carreau's model with the crudely obtained parameters as explained above.

Figure 13 shows the viscosity at start of steady shear flow for the PB melt at 298 K, and the model predictions. The two largest shear rates (0.198 and 0.79 rad $s^{-1}$) were obtained with a cone angle of 1.2° and the other shear rates with a cone angle of 6°. The plate diameter was 20 mm in every case. There is no apparent cone angle effect and furthermore there is no visible stress overshoot in this experiment.

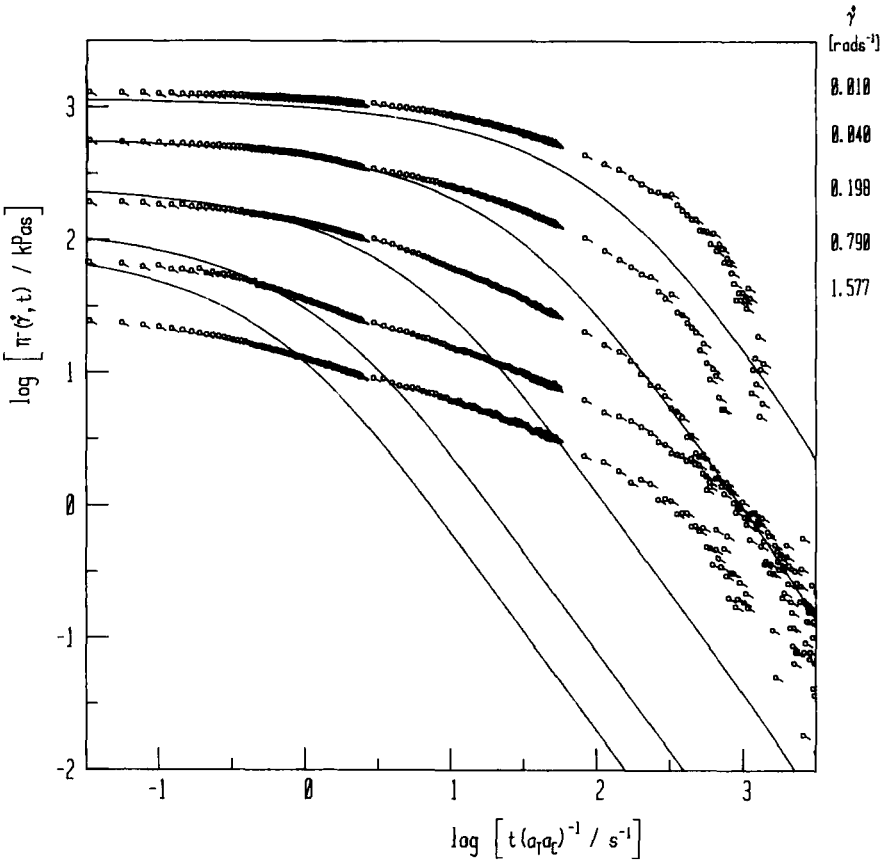


FIGURE 15 Viscosity at cessation of steady shear flow *vs.* time, PB melt, 298 K. Shear rate: 0.01–1.6 rad $s^{-1}$. Lines are predictions of Carreau model.

The first normal stress coefficient at start of steady shear flow is shown in Figure 14. Here the largest shear rate measurement (filled points 1.577 rad $s^{-1}$) was obtained with a cone angle of 1.2°, the others with a cone angle of 6°. A large discrepancy appears between measurements with different cone angles.

The viscosity and first normal stress coefficient at cessation of steady shear flow and theoretical predictions are presented in Figures 15 and 16. Cone angle effects are again visible, although it can be concluded that the theory overestimates the nonlinearity of the PB melt.

We summarize the results of the transient experiments and their fit to the modified network theory, as follows: 1) torque measurements appear to be reliable at all cone angles investigated here (1.2 and 6 degrees), 2) thrust measurements are probably accurate for cone angles of 6 degrees or more and definitely inaccurate for cone angles of 1.2 degrees, 3) the quality of fit between

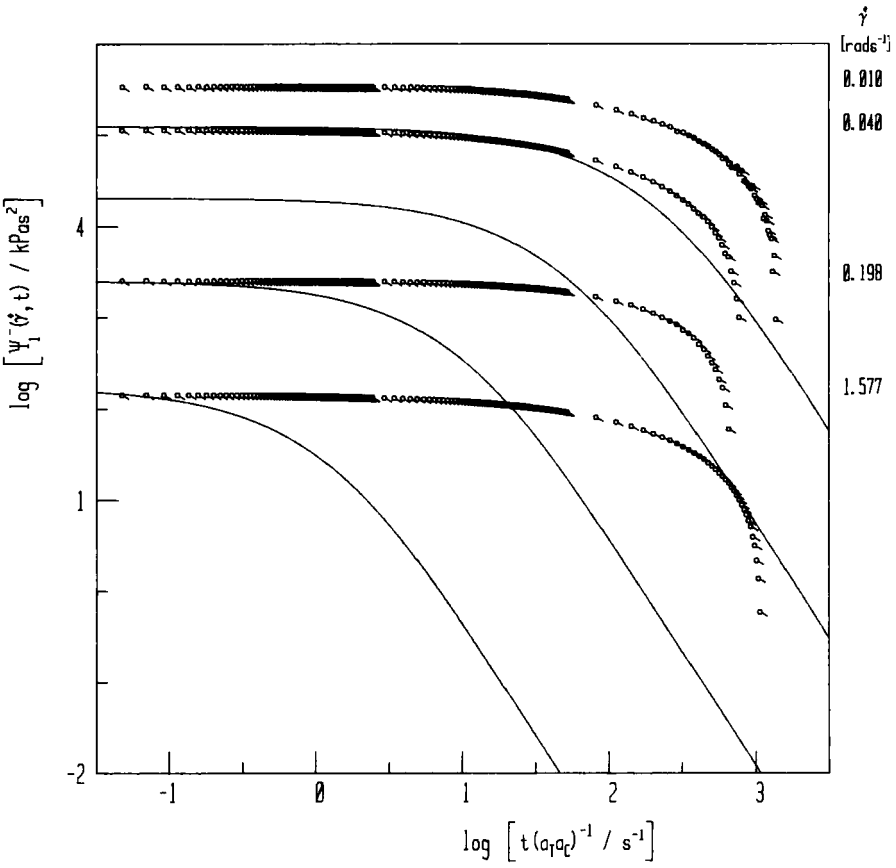


FIGURE 16 First normal stress coefficient at cessation of steady shear flow as in Figure 15.

theory and experiment is in the order $\eta^+ > \Psi_1^+ > \eta^- > \Psi_1^-$, 4) better signal-to-noise ratio is achieved when the drive motor is not in motion and 5) melt instability is a serious problem at the highest shear rates presented here.

It can be concluded that although empirical modifications of linear theories provide some degree of success, and the possibility of observing systematic changes in the complete viscoelastic behaviour of polymers is available, the real challenge lies in molecular theories which derive functional behaviour from clear, independently testable notions of molecular architecture.

## Acknowledgements

We thank the Deutsche Forschungsgemeinschaft for financial support of this work. We are most grateful to Professor A. S. Lodge for constructive criticism of the manuscript and to Professors A. S. Lodge and J. Meißner for fruitful discussions.

## References

1. A. S. Lodge, *Rheol. Acta* **7,** 379 (1968).
2. M. Doi and S. F. Edwards, *J. Chem. Soc., Faraday Trans. II* **74,** 1789, 1802, 1818 (1978).
3. C. F. Curtiss and R. B. Bird, *J. Chem. Phys.* **74,** 2016, 2026 (1981).
4. R. B. Bird, R. C. Armstrong and O. Hassager, *Dynamics of Polymeric Liquids, Vol. 1 Fluid Mechanics* (New York, Wiley, 1977).
5. P. E. Rouse, *J. Chem. Phys.* **21,** 1272 (1953).
6. J. D. Ferry, R. F. Landel and M. L. Williams, *J. Appl. Phys.* **26,** 359 (1955).
7. G. A. Alvarez and H.-J. Cantow, *Polym. Bull.* **4,** 383 (1981).
8. G. A. Alvarez and H.-J. Cantow, *Polym. Bull.* **7,** 137 (1982).
9. M. Kurata *et al., J. Polym. Sci.: Polym. Phys. Ed.* **12,** 849 (1974).
10. W. W. Graessley and S. F. Edwards, *Polymer* **22,** 1329 (1981).
11. N. W. Tschoegl, *Rheol. Acta* **10,** 582 (1971).
12. G. A. Alvarez and H.-J. Cantow, *Polym. Bull.* **7,** 51 (1982).
13. R. B. Bird, O. Hassager, R. C. Armstrong and C. F. Curtiss, *Dynamics of Polymeric Liquids, Vol. 2. Kinetic Theory* (New York, Wiley, 1977).
14. D. S. Pearson and W. E. Rochefort, *J. Polym. Sci.: Polym. Phys. Ed.* **20,** 83 (1982).
15. M. Yamamoto, *Japan. J. Appl. Phys.* **8,** 1252 (1969).
16. R. B. Bird, H. H. Saab and C. F. Curtiss, University of Wisconsin Rheology Research Center Report RRC78, April 1982.
17. P. J. Carreau, *Trans. Soc. Rheol.* **16**: 1, 99 (1972).
18. J. Meißner, *Rheol. Acta* **14,** 201 (1975).
19. A. S. Lodge, *Body Tensor Fields in Continuum Mechanics* (London, Academic Press, 1974).
20. D. Acierno *et al., J. non-Newt. Fluid Mech.* **1,** 125, 147 (1976); **2,** 271 (1977).
21. R. B. Bird and C. F. Curtiss, University of Wisconsin Rheology Research Center Report RRC 81, June 1982.